High precision quadrupole moment measurements of states up to $I=20\hbar$ in the yrast band of ^{158}Er

S. L. Shepherd,[1,*] J. Simpson,[2] A. Dewald,[3] P. Petkov,[3,4] P. J. Nolan,[1] M. A. Riley,[5] A. J. Boston,[1] T. B. Brown,[5] R. M. Clark,[6] P. Fallon,[6] D. J. Hartley,[5,†] S. Kasemann,[3] R. Krücken,[7] P. von Brentano,[3] R. W. Laird,[5] E. S. Paul,[1] and R. Peusquens[3]

[1]*Oliver Lodge Laboratory, Department of Physics, University of Liverpool, Liverpool, L69 7ZE, United Kingdom*
[2]*Central Laboratory of the Research Councils, Daresbury Laboratory, Daresbury, Warrington WA4 4AD, United Kingdom*
[3]*Institut für Kernphysik der Universität zu Köln, D-50937 Köln, Germany*
[4]*Bulgarian Academy of Sciences, Institute for Nuclear Research and Nuclear Energy, 1784 Sofia, Bulgaria*
[5]*Department of Physics, Florida State University, Tallahassee, Florida 32306*
[6]*Nuclear Science Division, Lawrence Berkeley National Laboratory, Berkeley, California 94720*
[7]*A.W. Wright Nuclear Structure Laboratory, Yale University, New Haven, Connecticut 06520*

(Received 22 October 2001; published 4 March 2002)

The lifetimes of excited states in the yrast band in ^{158}Er up to $I^{\pi}=20^{+}$ have been measured to high precision by means of the Gammasphere spectrometer using the coincidence recoil distance technique. The reaction ^{122}Sn(^{40}Ar,4n) at a beam energy of 185 MeV was used. The data were analyzed using the differential decay-curve method and transition quadrupole moments were extracted. The quadrupole moment was found to gradually increase by 15% of its 2^{+} value before the first $\nu i_{13/2}$ alignment, after which it drops to a constant level 90% of the 2^{+} value. Detailed comparisons are made with previous measurements and Ultimate Cranker calculations.

DOI: 10.1103/PhysRevC.65.034320 PACS number(s): 21.10.Re, 21.10.Tg, 23.20.Lv, 27.70.+q

I. INTRODUCTION

The $N=88$–92 nuclei have become classic cases for the study of normal deformed nuclear states at high angular momentum. Indeed, it is in the light mass ($A\sim160$) Dy and Er nuclei that the highest spin states in normal deformed nuclei have been observed (spin $\sim60\hbar$ and $E_{\rm excit}\sim30$ MeV) [1–13]. The studies of these nuclei have revealed a rich variety of nuclear structure information, in particular the mapping out of the nuclear shape with increasing angular momentum and the nature of the particle alignments that occur. In the weakly prolate $N=90$ region the first pair of particles that align with the axis of rotation is a pair of $i_{13/2}$ neutrons at spin $\approx12\hbar$ and the second a pair of $h_{11/2}$ protons at spin $\approx30\hbar$. The observation of many rotational bands in several nuclei in this region has enabled a detailed understanding of the quasiparticle excitations to be obtained. The action of the nuclear rotation and the quasiparticle alignments in general cause nuclear deformation changes. Indeed, at the highest spins dramatic shape changes occur in nuclei in this mass region. For example, the Er nuclei and some Dy isotopes [9,11,12] are textbook examples of the transition from prolate-collective to oblate noncollective shape at high spin [14–17]. In $^{156-159}$Er there are many examples of aligned oblate (band-terminating) states near the yrast line that show evidence of this transition [1–4].

In order to provide a more detailed understanding of the effects of band crossings and shape changes we have performed a high precision lifetime measurement on states in ^{158}Er. The lifetimes of states and corresponding transition probabilities are crucial quantities for testing nuclear models and they are a sensitive probe of the internal structure of the nucleus. The lifetimes were obtained from coincidence lifetime data using the recoil distance method [18]. The aim of the experiment was to measure the lifetimes of the excited states from spin 2^{+} up to spin 40^{+} to trace the collectivity of ^{158}Er from prolate-collective at low spin to oblate noncollective shape at high spin.

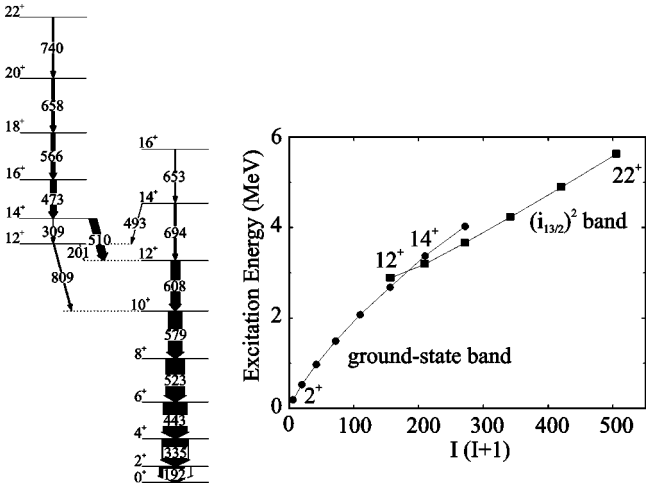

FIG. 1. Left. Partial low-spin level scheme of the even spin, positive parity states in ^{158}Er, taken from Refs. [19] and [20]. The width of the arrows indicates the relative intensity of the transitions. Right. Excitation energy as a function of $I(I+1)$ to illustrate the crossing at spin 12 between the ground-state band and $(i_{13/2})^2$ band in the yrast sequence of ^{158}Er.

*Present address: Urenco (Capenhurst) Ltd, Mass Spectrometry Laboratory, Capenhurst, Cheshire CH1 6ER, United Kingdom.

†Present address: Department of Physics and Astronomy, University of Tennessee, Knoxville, TN 37996.

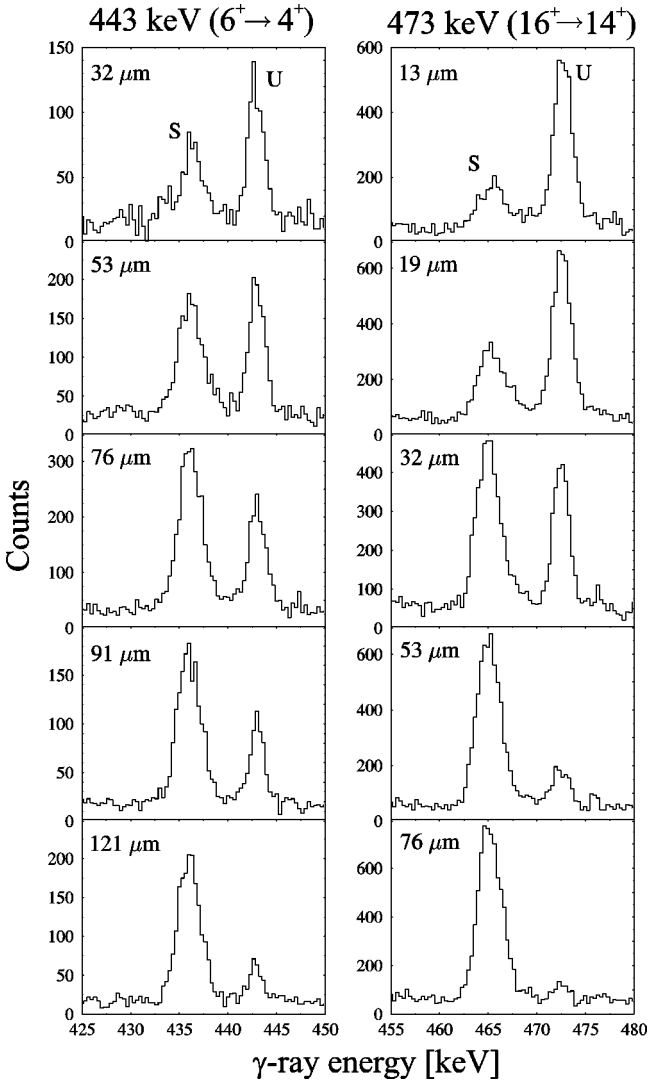

FIG. 2. The shifted (*S*) and unshifted (*U*) peaks at 142.6°, of the 443 keV ($6^+ \rightarrow 4^+$) and 473 keV ($16^+ \rightarrow 14^+$) transitions, for various target-to-stopper distances and obtained with a gate on the shifted component of the direct and an indirect feeding transition, respectively.

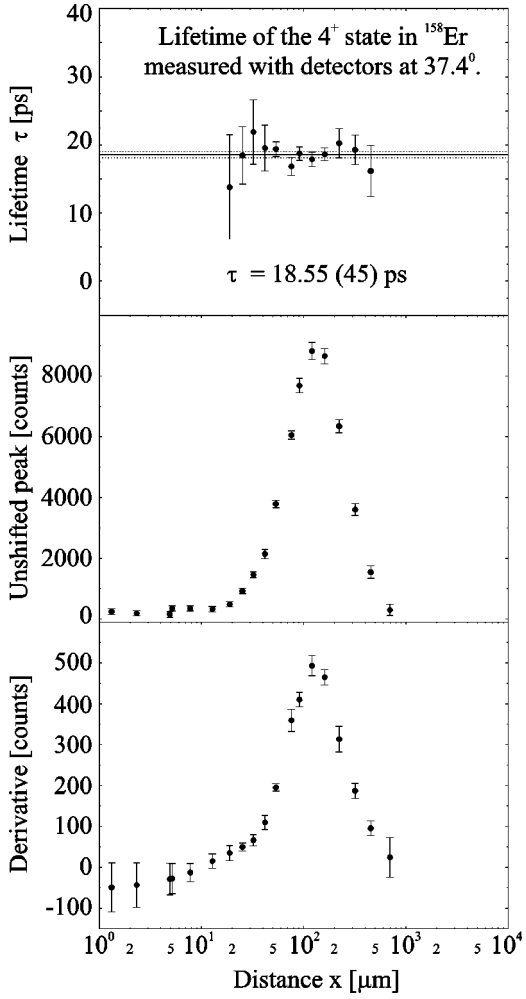

FIG. 3. Example of lifetime analysis according to the DDCM for the 335 keV ($4^+ \rightarrow 2^+$) transition. The data are measured with the detectors of ring 3 (37.4°). The bottom plot displays the denominator in Eq. (3) while the numerator is displayed in the middle. The resulting τ curve is shown in the top plot. Only the points of this curve that are used to obtain the average value 18.55 ± 0.45 (displayed also with a straight line and uncertainty limits) are presented. See text also.

The focus of this paper is the lifetimes of the low spin states in the yrast band in ^{158}Er up to 20^+ in order to examine the shape-change effect above and below the first $i_{13/2}$ neutron crossing in the yrast band [19,20] (cf. Fig. 1). Previous lifetime experiments by Oshima *et al.* [21] in 1986 using 6 Ge detectors were made for states in the yrast band up to $I^\pi \leqslant 22^+$. These measurements revealed a pronounced increase of the Q_t values for the yrast band transitions above the 4^+ state up to the $i_{13/2}$ neutron crossing at spin $12\hbar$. This enhanced collectivity was attributed to a change in β_2 and γ deformation. The higher spin states ($12^+ \leqslant I \leqslant 40^+$) were then measured by Beck *et al.* in 1988 [22], using the Hera array [23], which consisted of 21 Ge detectors. These data showed a gradual loss in collectivity along the yrast line of ^{158}Er from above the $i_{13/2}$ neutron crossing to the band-termination region, ≈ spin $40\hbar$. Similar significant reductions have also been reported in the neighboring $N=90$ isotones, e.g., Refs. [24] and [25].

The present experiment used the Gammasphere array [26], with 100 escape suppressed Ge detectors, to collect high statistics high-fold coincidence data. This enables coincidence lifetime analysis methods to be performed on the yrast band, with accuracies significantly better than previous measurements. This allows a stringent test of theoretical calculations, which can lead to a better understanding of the mechanism responsible for any shape-change effect. Detailed comparisions are made with the Ultimate Cranker calculations [27], which provide the most detailed theoretical analysis to date of the shape evolution with spin of ^{158}Er.

II. EXPERIMENTAL DETAILS

High spin states in the nucleus ^{158}Er were populated using the reaction ^{122}Sn(^{40}Ar,4*n*) at a beam energy of 185 MeV.

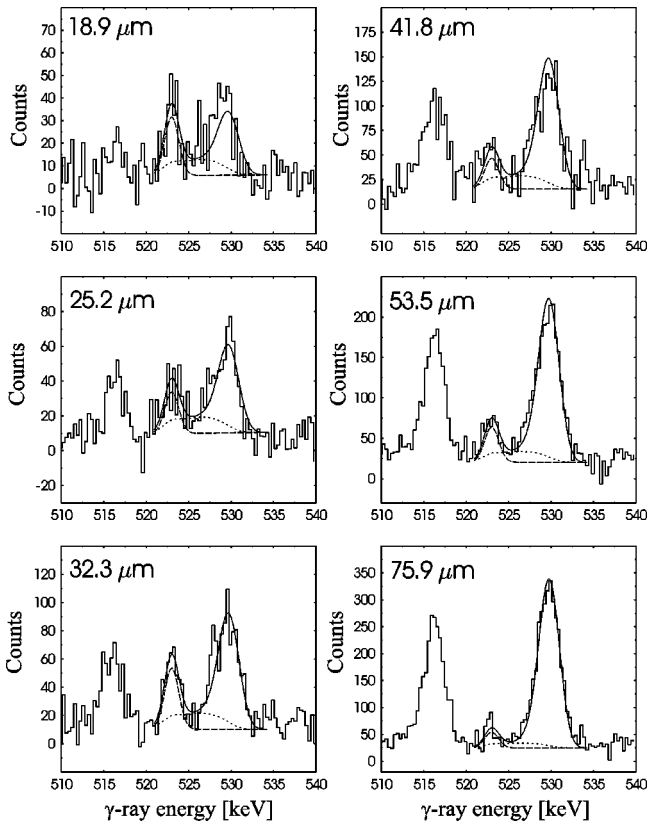

FIG. 4. Example of the analysis of spectra taking into account the DSA effect due to the finite slowing-down time of the recoils in the stopper. The spectra show the 523 keV ($8^+ \rightarrow 6^+$) transition observed at 50.1° gated by the 579 keV ($10^+ \rightarrow 8^+$) transition at 50.1°. At the indicated distances, the full line represents the fit of the line shape while the short-dashed line is the DSA contribution. The background and the unshifted peak are represented by a long-dashed line. The reduced $\chi^2 = 1.03$ of the fit at all distances is 10% smaller than the value obtained without taking into account the DSA effect. See text also.

The beam was provided by the 88-Inch Cyclotron of the Lawrence Berkeley National Laboratory. The target material consisted of a 1.25 mg/cm^2 ^{122}Sn (enriched to 92.25%), which was evaporated on an 1.68 mg/cm^2 Ta backing. The recoils, leaving the target with a velocity of 1.98% of the velocity of light, c, were stopped in a 10.5 mg/cm^2 Au foil. The target and stopper foils were mounted in the plunger apparatus of the University of Köln [28], which has been designed specifically for coincidence recoil distance lifetime measurements. This apparatus is equipped with an automatic regulation system of the target-to-stopper distance to correct for thermal drifts of the target foil induced by the beam. The capacitance between the target and stopper foils serves as a control signal for the regulation and is continuously monitored. The plunger apparatus [28] was mounted in the center of Gammasphere [26], the latter being used to efficiently detect the deexciting γ radiation. The Ge detectors in Gammasphere are arranged in 17 rings at the same angle with respect to the beam axis. For the analysis, only detectors where significant Doppler shifts were observed were used. These were the 5 detectors at 17.3°, 5 at 31.7°, 5 at 37.4°, 10 at 50.1°, 5 at 58.3°, 5 at 69.8°, 5 at 110.2°, 5 at 121.7°, 10 at 129.9°, 5 at 142.6°, 5 at 148.3°, and 5 at 162.7°.

During the experiment, data were taken at 19 different distances ranging from 1.3 to 697 μm with respect to electrical contact of the two foils. A total of 4.2×10^9 triples and higher-fold events were collected. An energy and efficiency calibration was performed with ^{152}Eu and ^{133}Ba radioactive sources. After shift correction of the detectors, these data were sorted into γ-γ coincidence matrices. Normalization factors for the different distances were derived using the coincident events corresponding to pairs of strong transitions in the ground-state band.

In order to eliminate the problem of accounting for observed and unobserved (side) feeding, spectra were generated by setting the gate on the Doppler-shifted component of a transition that directly or indirectly feeds the level of interest. This approach is now possible due to the high statistics that can be collected using a modern γ-ray spectrometer like Gammasphere. To illustrate the quality of the data obtained in this way, representative spectra are shown in Fig. 2.

III. DATA ANALYSIS

For the data analysis, the differential decay-curve method (DDCM) [29,30] was employed. Referring the reader for more details to the quoted works, here we only present the main points. The lifetime $\tau(x)$ of the level of interest at each target-to-stopper distance x is obtained from

$$\tau(x) = \frac{\{C_s, A_u\} - \alpha\{C_s, B_u\}}{(d/dx)\{C_s, A_s\}} \frac{1}{v}, \tag{1}$$

where

$$\alpha = \frac{\{C_s, A_u\} + \{C_s, A_s\}}{\{C_s, B_u\} + \{C_s, B_s\}}. \tag{2}$$

Here, v is the mean velocity of the recoils, and the quantities in braces are the number of events corresponding to detection of the Doppler-shifted (s) or the unshifted (u) components of the γ-ray transitions involved in the analysis. The transition A depopulates the level of interest whose lifetime has to be determined and which is fed directly by the transition B. The gate is set on the s component of the transition C that lies higher in the cascade above the level of interest. More general expressions for the derivation of $\tau(x)$ than Eq. (1), where it is implied that only one feeding path connects the levels depopulated by the transitions A, B, and C, can be found in Refs. [29] and [30]. In the case of a gate set on a direct feeder, Eq. (1) reduces to

$$\tau(x) = \frac{\{B_s, A_u\}}{(d/dx)\{B_s, A_s\}} \frac{1}{v}. \tag{3}$$

The derivative in the denominator of Eqs. (1) and (3) is derived by fitting piecewise with polynomials the gated decay curve of the shifted component of the transition A (i.e., the quantities $\{C_s, A_s\}$ or $\{B_s, A_s\}$, respectively). Using the equations above, the lifetime τ of the level of interest can be

TABLE I. The mean lifetime values obtained in the present work compared with earlier data. The $\langle\tau\rangle$ values are derived with a standard analysis while the τ_{corr} ones are the values obtained with a correction for DSA effects when the standard values are smaller than 2.5 ps. See text also.

I^{π}	$E_{\gamma}(I\rightarrow I-2)$ (keV)	$\langle\tau\rangle$ (ps)	τ_{corr} (ps)	Earlier data for τ (ps)
2^+	192	341±10		371±20 [21]
4^+	335	18.9±0.5		20.4±0.7 [21]
6^+	443	3.6±0.2		3.9±0.4 [21]
8^+	523	1.10±0.03	1.36±0.08	1.20±0.23 [21]
10^+	579	0.78±0.06	1.08±0.12	0.68±0.19 [21]
12^+	608	0.47±0.04	0.73±0.09	0.6±0.5 [21]
				$<$ 0.67 [22]
14^+	510	4.9±0.4		3.7±0.4 [21]
				$4.4^{+1.9}_{-0.9}$ [22]
16^+	473	3.3±0.3		3.6±0.3 [21]
				$2.4^{+0.8}_{-0.4}$ [22]
18^+	566	0.99±0.12	1.28±0.20	1.6±0.3 [21]
				$1.3^{+0.3}_{-0.3}$ [22]
20^+	658	0.44±0.09	0.66±0.14	$1.13^{+0.22}_{-0.19}$ [21]
				$0.78^{+0.15}_{-0.09}$ [22]

determined at every target-to-stopper distance. The obtained values of τ (the τ curve) should not depend on the distance at which they have been determined and correspondingly lie on a horizontal straight line when the lifetime is plotted versus distance. A deviation from such behavior immediately indicates the presence of systematic errors in the analysis. For the derivation of the mean value of the lifetime, not all points of the τ curve are used but only these which are reliably

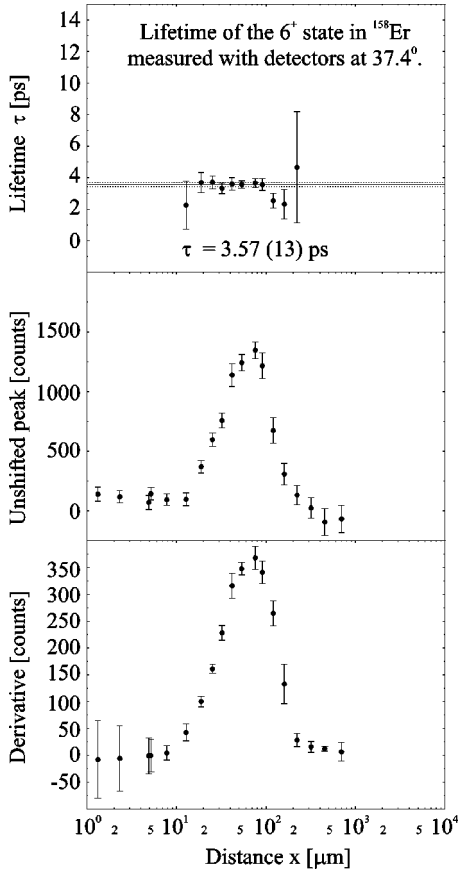

FIG. 5. Determination of the lifetime of the 6^+ state measured with the detectors at 37.4°. See also the caption to Fig. 3 and text.

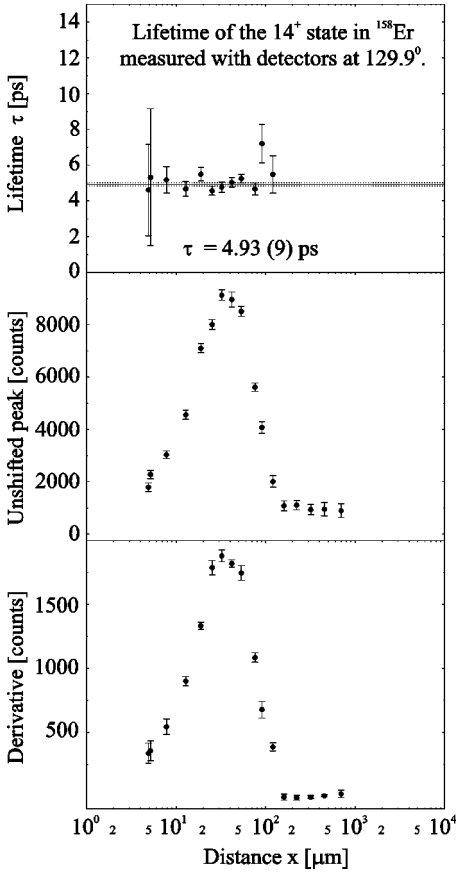

FIG. 6. Determination of the lifetime of the 14^+ state measured with the detectors at 129.9°. See also the caption to Fig. 3 and text.

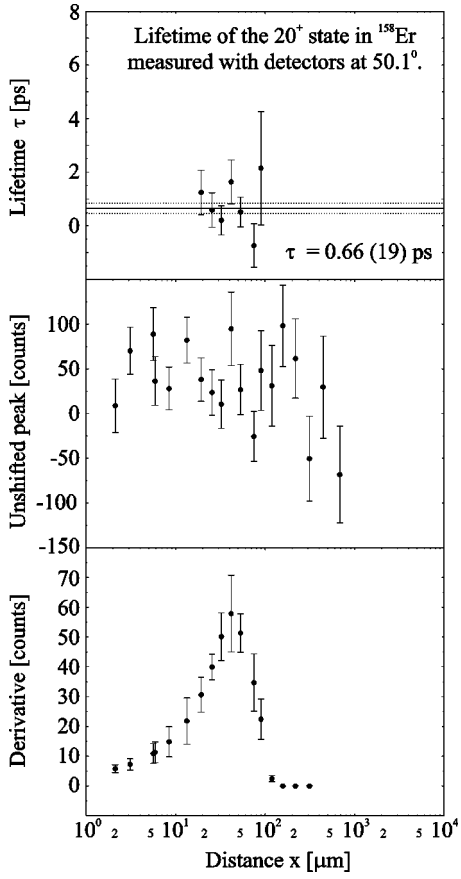

FIG. 7. Determination of the lifetime of the 20^+ state measured with the detectors at 50.1°. See also the caption to Fig. 3 and text.

defined, i.e., lie within the so-called region of sensitivity. Usually, this region covers the interval of distances where the quantities participating in the right-hand side (r.h.s.) of Eqs. (1) and (3) are not too small. Figure 3 shows the numerator and denominator of Eq. (3) as well as the resulting τ curve for the 4^+ state of ^{158}Er. The data are measured with the detectors of ring 3 and the gate is set on the shifted component of the direct feeding transition of 443 keV. Further examples of lifetime determination can be found in the next section (Sec. IV).

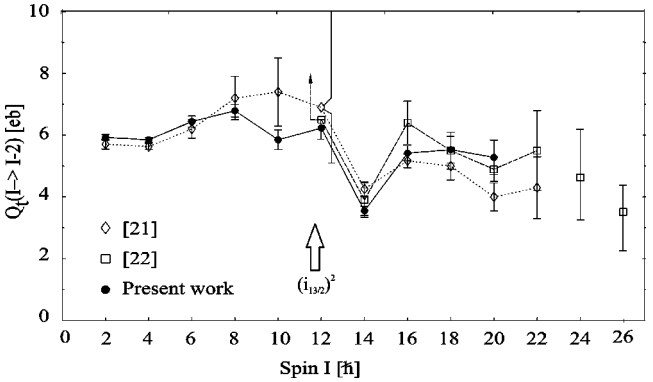

FIG. 8. The transitional quadrupole moments plotted as a function of spin, for the new and previous τ values. The position of the aligned neutron $(i_{13/2})^2$ crossing is indicated.

In practice, the analysis was performed by considering separately the coincidence data taken with the detectors belonging to the different rings of Gammasphere. To investigate a given level, gates on a feeding transition were set in the γ-γ matrices at all rings where contaminants or other problems did not disturb the gated spectra. Then, the spectra corresponding to every ''gated'' ring were summed up and the resulting spectrum analyzed. With six forward and six backward rings, this means that (maximum) twelve lifetime values were determined for both direct and indirect feeder cases. The final value of the lifetime τ was derived by averaging the individual results.

A more careful consideration of the data is necessary in the cases where the lifetimes determined are comparable with or smaller than the mean slowing-down time of the ^{158}Er ions in the gold stopper. During the slowing-down time, which takes place in about 1.3 ps, the emission of deexciting γ rays leads to the appearance of a complementary [Doppler-shift attenuated (DSA)] component in the total line shape that was treated according to the technique described in Ref. [31], where further details can be found. Examples of the application of this technique are shown in Fig. 4 for the case of the 523 keV $8^+ \rightarrow 6^+$ transition. The spectra taken at all distances are fitted simultaneously until the best reproduction of the data is obtained for a particular value of

TABLE II. $B(E2)$, Q_t, and β_2 values derived in the present work.

I^π	$E_\gamma(I \rightarrow I-2)$ (keV)	$B(E2)$ (e^2b^2)	$B(E2)$ (Weisskopf units)	Q_t (eb)	β_2
2^+	192	0.70±0.02	138±4	5.93±0.09	0.263±0.004
4^+	335	0.97±0.03	191±5	5.85±0.08	0.259±0.002
6^+	443	1.30±0.07	255±14	6.44±0.18	0.285±0.008
8^+	523	1.51±0.09	297±18	6.79±0.20	0.299±0.009
10^+	579	1.15±0.13	226±25	5.85±0.32	0.259±0.014
12^+	608	1.33±0.16	262±32	6.23±0.38	0.276±0.016
14^+	510	0.44±0.04	86±7	3.55±0.15	0.160±0.007
	309	0.47±0.05	93±10	3.69±0.20	0.166±0.009
16^+	473	1.03±0.09	202±18	5.42±0.24	0.241±0.011
18^+	566	1.08±0.17	213±33	5.53±0.43	0.246±0.019
20^+	658	0.99±0.21	194±41	5.28±0.56	0.235±0.024

TABLE III. Result of a two-level mixing calculation for the 12^+ and 14^+ states of band I and II shown in Fig. 1. In order to calculate the transition probabilities Q_t values of 6.8 eb and 5.4 eb were used for the pure $(14\rightarrow12)$ intraband transitions of the ground-state band and *s* band, respectively.

Interaction V (keV)	State	Mix. ampl. ground-state band	Mix. ampl. *s* band
65	12_I^+	0.343	0.939
	12_{II}^+	0.939	−0.343
50	14_I^+	−0.347	0.938
	14_{II}^+	0.938	0.347

Transition	$B(E2)_{cal}$ (e^2b^2)	$B(E2)_{expt}$ (e^2b^2)
$14_I\rightarrow12_I$	0.468	0.47(5)
$14_I\rightarrow12_{II}$	0.449	0.44(4)
	Calc.	Expt.
$\frac{B(E2;14_{II}\rightarrow12_{II})}{B(E2;14_{II}\rightarrow12_I)}$	1.8	1.7 ± 0.2

the lifetime τ. In this way, correction factors were derived for the lifetimes obtained with the conventional DDCM analysis. These factors increase to 60% for the shortest lifetimes derived in the present work (see next section), and on the other hand, are not needed for lifetimes larger than 2.5 ps. They were determined using stopping powers for ^{158}Er ions in gold derived from the tables of Northcliffe and Schilling [32] with corrections for the atomic structure of the medium [33,34]. More details on our approach for the Monte Carlo simulation of the slowing down of the recoils can be found in Ref. [31] and the references quoted therein. The correction factors for the DSA effects remain stable when the stopping powers used for their derivation are decreased or increased with 20%.

IV. RESULTS

The results of the lifetime analysis according to the DDCM are summarized in Table I. Examples of lifetime determination are shown in Figs. 5, 6, and 7. The 20^+ state is the highest-lying state whose lifetime could be determined, using this coincidence technique, in the present experiment. The τ data obtained at different angles were carefully averaged and the values affected by systematic errors were rejected. The quoted statistical errors were derived as a result of the averaging procedure. A comparison with earlier data on the lifetimes in ^{158}Er reveals a reasonable overall agreement and points to the better precision characterizing the present results. The lifetimes obtained in the present work for the 4^+ and 10^+ states differ from the previous data [21] by more than one standard deviation and have a better precision. At 14^+ and 20^+, the present data show better agreement with the lifetimes obtained by Beck *et al.* [22] and deviate from those deduced in Ref. [21]. We note that the use of the coincidence technique with setting gates on feeding transitions ensures a higher degree of reliability to the newly obtained data.

The τ values deduced in this work were used to derive values of the reduced transition probabilities $B(E2;\ I\rightarrow I-2)$, the transitional quadrupole moments Q_t, and the β_2 deformation parameters. These quantities are displayed in Table II. The Q_t's were calculated using the relation

$$B(E2)=\frac{5}{16\pi}Q_t^2|\langle IK20|I-2K\rangle|^2 \tag{4}$$

and assuming $K=0$. Their values were employed to derive the ellipsoidal deformation parameter β_2 by using the expression

$$Q_t=\frac{3}{\sqrt{5\pi}}ZR_0^2\beta_2\left(1+\frac{1}{8}\sqrt{\frac{5}{\pi}}\beta_2\right), \tag{5}$$

where Q_t is in electron barns (eb) if the squared mean nuclear radius R_0^2 is in barns.

V. DISCUSSION

The yrast band of ^{158}Er undergoes the first $i_{13/2}$ neutron [19] crossing at spin $12\hbar$, and the lifetimes measured in this work (see Table I), cover the region below and above this crossing. A plot of transition quadrupole moment as a function of spin, for the previous [21,22] and new τ values, is displayed in Fig. 8. All the values displayed in Fig. 8 show a slight increase ($\approx$15%) in collectivity up to spin $8\hbar$ just below where the $(i_{13/2})^2$ neutron band crossing starts to take place. This is typical of nuclei in the $N=88$ and 90 region e.g., Refs. [35–38] and has been interpreted as being due to a centrifugal stretching of the nucleus with increasing spin. Theoretical calculations [39] have revealed that such nuclei have a very shallow minimum in their potential-energy surfaces. This makes them susceptible to deformation driving influences. The stretching of the nucleus with increasing spin can simply be attributed to the Fermi surface lying very close

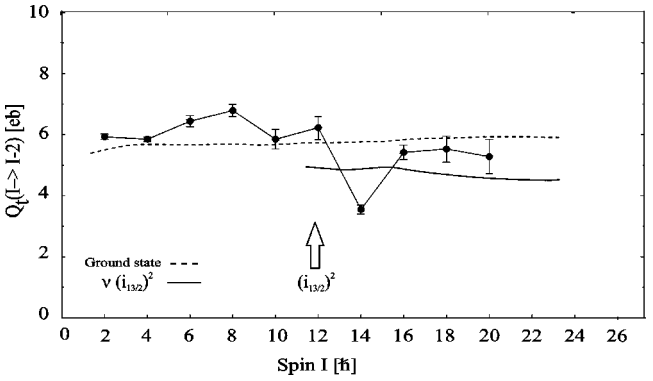

FIG. 9. Theoretical transitional quadrupole moments, taken from Ref. [37] for the ground state (dashed line) and the neutron $(i_{13/2})^2$ configuration (full line), and the present experimental results. The position of the aligned neutron $(i_{13/2})^2$ crossing is indicated.

to the deformation driving $i_{13/2}$ [651]3/2 ([660]1/2) orbital. At spin 10^+ to 14^+, where the the $(i_{13/2})^2$ neutron band crossing takes place, the results in Fig. 8 show a reduction in the quadrupole moment. This sudden drop is particularly apparent for the $14^+ \rightarrow 12^+$ transition. Sudden deviations may indeed be expected in the crossing region between the two bands. In order to investigate this further we have performed a two-band mixing calculation for the 12^+ and 14^+ states of the ground and $(i_{13/2})^2$ or *s* band. We write the state vectors of the observed states, e.g., for the 12^+ levels, as follows:

$$|12_{\mathrm{I}}\rangle = \alpha|12_g\rangle + \beta|12_s\rangle,$$

$$|12_{\mathrm{II}}\rangle = \beta|12_g\rangle - \alpha|12_s\rangle,$$

where the notation of the observed (mixed) states is the same as in Fig. 1, with states labeled I in the left-hand band and II the right-hand band. *g* and *s* indicate the states belonging to the unmixed ground-state band and *s* band, respectively. Irrespective of the interaction strengths v_{12} and v_{14} of the 12^+ and 14^+ states, respectively, the $B(E2)$ ratios $B(E2;14_{\mathrm{II}} \rightarrow 12_{\mathrm{II}})/B(E2;14_{\mathrm{II}} \rightarrow 12_{\mathrm{I}})$ and $B(E2;14_{\mathrm{I}} \rightarrow 12_{\mathrm{II}})/B(E2;14_{\mathrm{I}} \rightarrow 12_{\mathrm{I}})$ are equal if one assumes the same transition matrix elements in the ground and *s* band. Experimentally we find $B(E2;14_{\mathrm{II}} \rightarrow 12_{\mathrm{II}})/B(E2;14_{\mathrm{II}} \rightarrow 12_{\mathrm{I}}) = 1.7$ and $B(E2;14_{\mathrm{I}} \rightarrow 12_{\mathrm{II}})/B(E2;14_{\mathrm{I}} \rightarrow 12_{\mathrm{I}}) = 0.9$. This indicates different transition matrix elements in the two bands for the transitions of interest, which is also supported by the measured $B(E2)$ values given in Table II. The transition quadrupole moments Q_t of the ground-state band increase with increasing spin before the band crossing. Assuming that this trend continues to higher spin, above the band crossing region, a value of $Q_t(14_g \rightarrow 12_g)$ of about 6.8 eb is obtained for the unmixed states. For the *s* band above the 16^+ state our data show rather constant Q_t values from which an average value of 5.4 eb is obtained. These Q_t values were used to calculate the transition probabilities between the mixed 12^+ and 14^+ states. The interaction strengths $v_{12} = 65$ keV and $v_{14} = 60$ keV was found to give the best agreement with the experimental values. The result of this calculation is summarized in Table III.

We consider that the mixing calculation is in reasonable agreement with the experiment. The interaction strengths $v_{12} = 65$ keV and $v_{14} = 60$ keV also agree with the value of 60 keV deduced from the cranked shell model calculations [40] and with the systematics of the values extracted in this region of nuclei [41]. In addition, the increase of the Q_t values with increasing spin in the ground-state band is supported by the mixing calculation.

The present lifetime results show that after the band crossing the quadrupole moment returns to $\approx 90\%$ of its value measured at low spin (2^+, 4^+) up to 20^+. The previous results indicate a gradual reduction in collectivity with increasing spin above the band crossing. Indeed, the measurements of Beck *et al.* [22], plotted to spin 26^+ in Fig. 8, show that the quadrupole moment decreases to just under 2 eb at spin 40^+.

In order to understand these results in more detail the data are compared with the Ultimate Cranker model that actually used ^{158}Er as a special initial test case [42]. These calculations used a cranked mean field potential with the inclusion of pairing in order to extract the deformation properties in different configurations. A complete description of the calculations can be found in Ref. [27].

The quadrupole moments obtained from the calculations reported in Ref. [42] are reproduced in Fig. 9, along with the experimental values from the present work. The calculated values correspond to the ground-state configuration and the $(i_{13/2})^2$ neutron configuration. The calculation predicts that the ground-state band prefers a deformation of $\epsilon = 0.21$ and $\gamma = -6°$ and the $(i_{13/2})^2$ neutron configuration to have a fairly constant deformation with $\epsilon = 0.21$ and $\gamma = 7° - 10°$. The Q_t values are calculated to be larger below the $(i_{13/2})^2$ crossing than above and the values for the two configurations are roughly constant as a function of spin. The high accuracy of the experimental measurements enables a detailed comparison with the calculations. Indeed, there is a discrepancy below the crossing where the experimental values show a slight increase as a function of spin and above the crossing the data have a consistently higher Q_t than the calculated values.

It would be interesting to extend these highly accurate measurements to higher spin to investigate in greater detail the significant reduction of the experimental quadrupole moment with spin, reported by Beck *et al.* [22], and the dramatic shape change that takes place in the yrast band of ^{158}Er at spin 40^+ [1]. In this way, state-of-the-art theoretical calculations, like the Ultimate Cranker, could be investigated over a large spin range where many configuration and pairing changes occur.

VI. SUMMARY

The highest precision lifetime measurements to date of the yrast states in ^{158}Er up to 20^+ have been obtained using the recoil distance method. The Gammasphere γ-ray spectrometer array and the University of Köln plunger apparatus were used to obtain high statistics coincidence data.

The results agree with the general trends observed in previous studies with a slight increase in transition quadrupole moment before the first $i_{13/2}$ neutron band crossing. However, unlike previous studies where the quadrupole moment decreased monotonically, it was found that after the band crossing, the transition quadrupole moment was rather constant with values $\approx 90\%$ of those at low spin. This difference between the various measurements may be attributed to the superior technique of the differential decay-curve method that eliminates feeding problems. The new results have been compared with the Ultimate Cranker model that used ^{158}Er as its initial test example. These calculations also predict a lower and roughly constant quadrupole moment above the crossing, but with a reduction factor twice that observed experimentally.

ACKNOWLEDGMENTS

Support for this work was provided by the U.K. Engineering and Physical Sciences Research Council EPSRC, the USA National Science Foundation, and the State of Florida, the U.S. DOE under Grant Nos. DE-FG02-91ER-40609 and DE-AC03-76SF00098 as well as by the BMBF under Contract No. 06 OK958. S.L.S. acknowledges financial support from the EPSRC. J.S. and M.A.R. acknowledge the receipt of a NATO Collaborative Research Grant.

[1] J. Simpson *et al.*, Phys. Lett. B **B327**, 187 (1994).
[2] S.J. Gale *et al.*, J. Phys. G **21**, 193 (1995).
[3] F.S. Stephens, M.A. Deleplanque, R.M. Diamond, A.O. Macchiavelli, and J.E. Draper, Phys. Rev. Lett. **54**, 2584 (1985).
[4] F.G. Kondev *et al.*, J. Phys. G **25**, 897 (1999).
[5] M.A. Deleplanque, J.C. Bacelar, E.M. Beck, R.M. Diamond, J.E. Draper, R.J. McDonald, and F.S. Stephens, Phys. Lett. B **B193**, 422 (1987).
[6] M.A. Riley, J.D. Garrett, J. Simpson, and J.F. Sharpey-Schafer, Phys. Rev. Lett. **60**, 553 (1988).
[7] J. Simpson, M.A. Riley, A.N. James, A.R. Mokhtar, H.W. Cranmer-Gordon, P.D. Forsyth, A.J. Kirwan, D. Howe, J.D. Morrison, and J.F. Sharpey-Schafer, J. Phys. G **13**, L235 (1987).
[8] M.A. Riley *et al.*, J. Phys. G **16**, L67 (1990).
[9] R. Vlastou *et al.*, Nucl. Phys. **A580**, 133 (1994).
[10] H.W. Cranmer-Gordon *et al.*, Nucl. Phys. **A465**, 506 (1987).
[11] W.C. Ma *et al.*, Phys. Rev. Lett. **61**, 46 (1988).
[12] F.G. Kondev *et al.*, Phys. Lett. B **B437**, 35 (1998).
[13] J. Simpson *et al.*, Phys. Rev. C **62**, 024321 (2000).
[14] I. Ragnarsson, Z. Xing, T. Bengtsson, and M.A. Riley, Phys. Scr. **34**, 651 (1986).
[15] A.V. Afanasjev, D.B. Fossan, G.J. Lane, and I. Ragnarsson, Phys. Rep. **322**, 1 (1999).
[16] J. Simpson *et al.*, Phys. Rev. Lett. **53**, 648 (1984).
[17] M.A. Riley, J.D. Garrett, J.F. Sharpey-Schafer, and J. Simpson, Phys. Lett. B **B177**, 15 (1986).
[18] T.K. Alexander and A. Bell, Nucl. Instrum. Methods Phys. Res. **81**, 22 (1970).
[19] J. Simpson, P.A. Butler, P.D. Forsyth, J.F. Sharpey-Schafer, J.D. Garrett, G.B. Hagemann, B. Herskind, and L.P. Ekström, J. Phys. G **10**, 383 (1984).
[20] M.A. Riley, Ph.D. thesis, University of Liverpool (1984).
[21] M. Oshima, N.R. Johnson, F.K. McGowan, C. Baktash, I.Y. Lee, Y. Schutz, R.V. Ribas, and J.C. Wells, Phys. Rev. C **33**, 1988 (1986).
[22] E.M. Beck, H. Hubel, R.M. Diamond, J.C. Bacelar, M.A. Deleplanque, K.H. Maier, R.J. McDonald, F.S. Stephens, and P.O. Tjøm, Phys. Lett. B **B215**, 624 (1988).
[23] R.M. Diamond and F.S. Stephens, in *Proceedings of the Conference on Instrumentation for Heavy Ion Nuclear Research*, edited by D. Shapira, Vol. 7 of the Nuclear Science Research Conference Series (Harwood, New York, 1984), p. 301.
[24] N.R. Johnson *et al.*, Phys. Rev. C **53**, 671 (1996).
[25] H. Emling *et al.*, Phys. Lett. B **B217**, 33 (1989).
[26] I.Y. Lee, Nucl. Phys. **A520**, 641 (1990).
[27] T. Bengtsson, Nucl. Phys. **A496**, 56 (1989).
[28] A. Dewald *et al.*, Nucl. Phys. **A545**, 822 (1992).
[29] A. Dewald, S. Harissopulos, and P. von Brentano, Z. Phys. A **334**, 163 (1989).
[30] G. Böhm, A. Dewald, P. Petkov, and P. von Brentano, Nucl. Instrum. Methods Phys. Res. A **329**, 248 (1993).
[31] P. Petkov, D. Tonev, J. Gableske, A. Dewald, T. Klemme, and P. von Brentano, Nucl. Instrum. Methods Phys. Res. A **431**, 208 (1999).
[32] L.C. Northcliffe and R.F. Schilling, Nucl. Data Tables **A7**, 233 (1970).
[33] J.F. Ziegler and W.K. Chu, At. Data Nucl. Data Tables **13**, 463 (1974).
[34] J.F. Ziegler and J.P. Biersack, in *Treatise on Heavy-Ion Science*, edited by D.A. Bromley (Plenum, New York, 1985), Vol. 6, p. 95.
[35] R. M. Diamond, F. S. Stephens, W. H. Kelly, and D. Ward, Phys. Rev. Lett. **22**, 564 (1969).
[36] R. M. Diamond, F. S. Stephens, K. Nakai, and R. Nordhagen, Phys. Rev. C **3**, 344 (1971).
[37] L. L. Riedinger, Phys. Scr., T **T5**, 36 (1983).
[38] Ts. Venkova and W. Andrejtscheff, At. Data Nucl. Data Tables **26**, 93 (1981).
[39] S. Åberg, Phys. Scr. **25**, 23 (1982).
[40] R. Bengtsson, S. Frauendorf, and F.R. May, At. Data Nucl. Data Tables **35**, 15 (1986).
[41] G.B. Hagemann and I. Hamamoto, Phys. Rev. C **46**, 838 (1992).
[42] T. Bengtsson, Nucl. Phys. **A512**, 124 (1990).